Russian Geology and Geophysics © 2021, Novosibirsk State University
Available online in April 2021 *DOI: 10.2113/RGG20194156* *Geologiya i Geofizika*

Relationship between Selected Major, Minor, and Trace Elements in Iron Oxide–Copper–Gold Deposits, an Example from the Unique Sin Quyen Deposit (Lào Cai Province, North Vietnam)

H. Duong Van[a], C. Nguyen Dinh[b,✉], A. Piestrzyński[b], J. Pieczonka[b]

[a]*University of Mining and Geology (UMG), Hanoi, Vietnam*

[b]*AGH University of Science and Technology (AGH-UST), Krakow, Poland*

Received 14 November 2019; accepted 28 February 2020

Abstract—We study the relations between several selected elements present in the Sin Quyen IOCG deposit, Lào Cai, North Vietnam, and interpret the obtained correlations, especially with a coefficient higher than 0.7. The correlations with high coefficients are mainly observed for the elements belonging to the chalcophile group (Cu, Ag, Au, Te, and Bi) and for the relation between uranium and Ag, Au, Cu, Pb, and Bi. Although the S-, Fe-, and REE-bearing minerals are predominant in the studied deposit, no strong correlation between them and the other elements was observed, even with Cu. The phenomena are primarily explained based on the geochemical properties of the mentioned elements and the characteristics of IOCG deposits.

Keywords: Sin Quyen IOCG deposit; correlations; geochemistry

INTRODUCTION

The IOCG deposits are known as the deposits with the elevated contents of Cu, Au, Ag, REE, U, P, and Co. They are controlled structurally or stratigraphically and temporally and spatially associated with Na–Ca–K alteration (Barton, 2014). According to numerous scientists, the IOCG deposits might have formed as a consequence of (1) magmatic hydrothermal fluid activity, (2) metamorphic hydrothermal fluids derived from a crustal source at depth, and (3) terrestrial hydrothermal fluids circulated by intrusive or crustal heat (Hitzman et al., 1992; Groves et al., 2010). The mineral and chemical composition spectra of the IOCG deposits are very inhomogeneous even within one area (Li et al., 2014). The variety both in mineral composition and in ore distribution within a deposit might be connected with many periods of the magmatism activity and formation of geologic structures. The inhomogeneity is also reflected in variable ratios of different elements: Cu/Au, Au/Ag, and so on (Bonev et al., 2002; Zhu, 2016). Depending on the local geologic conditions, the IOCG deposits can be poor or rich in Fe, Cu, or other mentioned elements (Requia and Fontboté, 2000; Gandhi, 2003; Requia et al., 2003). Therefore not only can Fe or Cu be the main mined ores, but also Au, Ag, U or REE are valuable commodities.

There is an important role for geochemistry in the exploration workflow. Especially, for very broad distribution of trace elements around IOCG deposits, and these can be used to recognize 'halos' within mineral systems, also for deposits formed beneath a thick sediment surface (Fabris et al., 2015).

In geochemistry the stochastic dependences between different major and trace elements occurring in a deposit are often analyzed, because the relations can enable us to understand and to explain some unexpected phenomena or discover some valuable rules. For example, in the ores of high-Fe grade, there is often low Ti with variable Cu, Au, Ag, and REE, or in allanites-Ce the REE concentration is inversely proportional to the Ca contents (Zhao and Zhou, 2011; Barton, 2014). Silver contents in multistage deposits (skarn, massive sulfides, and black shale) increase abruptly in later low-temperature assemblages regardless of the deposit type (Gas'kov, 2017). Letnikova et al. (2011) used geochemical correlations of different oxides to reconstruct the geodynamic processes of forming deposits in the Tuva–Mongolian Massif. In the placer gold deposits in the East of the Siberian Platform, the Ag content decreases, and Cu has an increasing tendency with increasing Au fineness (Nikiforova et al., 2018).

Although the Sin Quyen IOCG deposit was investigated by several scientists, they focused principally on the geologic structure, ore crystallization ages, and occurrence of the specific minerals (Ta, 1975; McLean, 2001; Ishihara et al., 2011; Gas'kov et al., 2012; Li and Zhou, 2018; Piec-

✉ Corresponding author.
E-mail address: cnd@agh.edu.pl (C. Nguyen Dinh)

zonka et al., 2019). The correlation coefficients between some elements in the Sin Quyen IOCG deposit were also estimated by Gas'kov et al. (2012), but the correlations were not interpreted or considered very little. In this paper we present some interesting characteristic correlations between chalcophile elements (Cu, Ag, Au, Pb, Bi, Te, and Zn), the siderophile elements (Fe, Co, and Ni), and the lithophile elements as well as between the radioactive elements (Th and U) and major ore elements Cu, Au, Ag, and REE. In the Sin Quyen IOCG deposit, the sulfur- and iron-bearing minerals are dominating, but there is no correlation between these elements and others, even with Cu; however, the phenomena will also be considered.

STUDY AREA

The Sin Quyen IOCG deposit is located in the Lào Cai Province, 300 km to the northwest of Hanoi and one km from the Red River, which is the natural boundary with China (Fig. 1). The coordinates of the deposit are 22°37′20″ N and 103°48′00″ E, and its area is 200 ha. From the geological point of view, the deposit is within the Red River zone in the west of the Fanxipan belt. The Fanxipan belt divides North Vietnam into the South China and Indochina blocks and extends in the NW–SE direction, being nearly 300 km long in the Vietnam territory. The Fanxipan belt is composed of a high-grade metamorphic complex zone. The Red River zone is composed of the Suối Chiêng and Sin Quyen formations

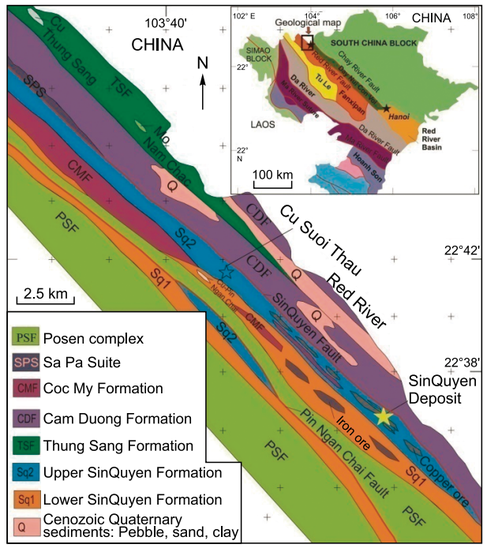

Fig. 1. Localization of the Sin Quyen deposit on the geological sketch map of North Vietnam.

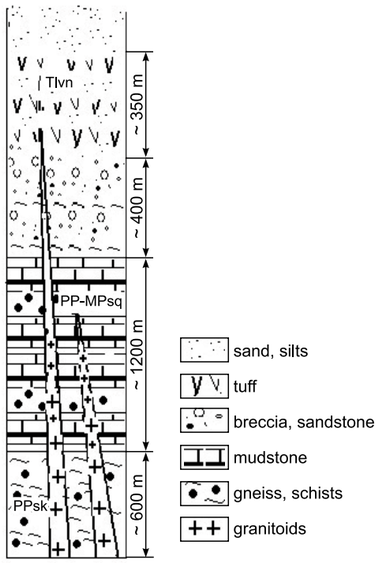

Fig. 2. Schematic illustration of the rock formation in the Sin Quyen region.

(Fig. 2). The Suối Chiêng Formation (nearly 600 m in thickness) is composed principally of Proterozoic terrigenous sediments and granitic gneiss, biotite–amphibole gneiss, and biotite schists. The Suối Chiêng Formation is covered conformably by the Sin Quyen Formation, 1200 m in thickness. From the facies point of view, the Sin Quyen Formation is divided into the lower and upper units. In the lower unit, there is gneiss composed of biotite, muscovite, and graphite quartz, while the composition of the upper unit is similar, but without graphite. The Sin Quyen Formation is intruded

Fig. 3. Cross section of the ore body (photo, 2015, looking in the NW direction).

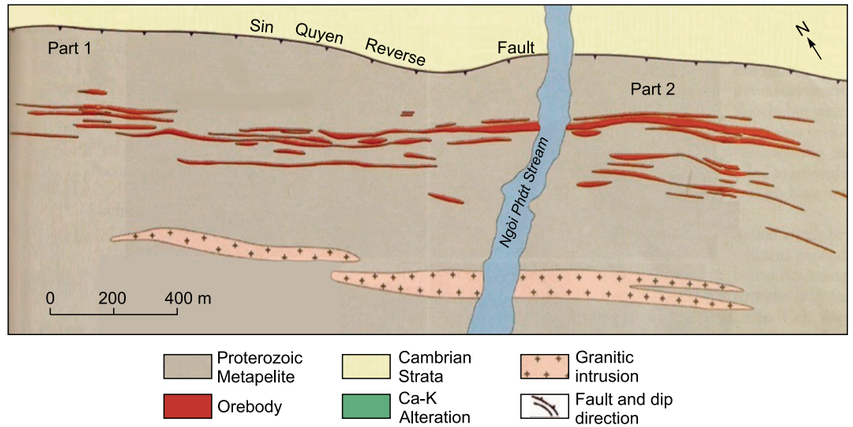

Fig. 4. Geological sketch map of the Sin Quyen deposit, modified after (Ta, 1975).

by several mafic intrusive dikes or lenses and is overlain conformably by the Cambrian-Ordovician Cam Duong sediments (McLean, 2001; Ishihara et al., 2011; Gas'kov et al., 2012).

The ore bodies of the Sin Quyen IOCG deposit are principally hosted in the Sin Quyen Formation. They occur as the lenses several tens of meters thick and up to a few hundred meters long, trending NW–SE and dipping near-vertically (70–90°) (Fig. 3). The major ore minerals are Au- and Ag-rich copper and iron sulfides (chalcopyrite, pyrite, and pyrrhotite) and iron oxides (magnetite and hematite). The average grade of Cu, LREE, and Au is equal to 0.9 wt.%, 0.7 wt.%, and 0.44 ppm, respectively. With the Cu grade being 0.9 wt.% and the maximum depth of the ore body occurrence being 350 m b.s.l., the calculated copper resource of the Sin Quyen IOCG deposit amounts to about 90 Mt (McLean, 2001; Pham, 2015). The deposit has an uncommon ore composition and is divided horizontally into two parts (Fig. 4). The first one is widespread in the central and eastern areas; in this part the main ore minerals are chalcopyrite, pyrrhotite, and pyrite, which make up about 90% of the ore composition. The second part is localized in the western area, where the major minerals are magnetite, pyrite, chalcopyrite, and pyrrhotite, constituting from a few percent to 50% of ore (McLean, 2001; Gas'kov et al., 2012). Because of the occurrence of the large fracture system, the oxidized zone is clearly observed in the upper part at a depth of about 100 m below the Earth's surface (Fig. 5) (Pieczonka et al., 2019).

According to Li et al. (2017), there were four principal mineralization stages in the deposit region: (1) the paragenetic sequence, including the sodic alteration, which happened in the Proterozoic; (2) the calcic–potassic alteration and associated Fe–REE–(U) mineralization took place duving the Neoproterozoic (841 to 836 Ma); (3) Cu–Au mineralization (probably at 500 Ma) (Pieczonka et al., 2015, 2019); (4) metamorphism took place at 30 Ma, and the sulfide–(quartz–carbonate) veins were mostly established. The mineralization of the Sin Quyen deposit basically falls within the age range of the Neoproterozoic igneous rocks 860–740 Ma) (Li et al., 2017).

MATERIALS AND METHODS

In November 2014 at the Sin Quyen IOCG deposit, 50 solid samples were collected from massive ores, host rocks, reservoir sediments, Cu- and Fe-concentrates, and waste dumps. The localization of the sampling places is shown in Fig. 6.

All the collected samples were analyzed using an optical microscope at AGH University of Science and Technology (AGH-UST). Based on the results of the microscope analy-

Fig. 5. View of weathered zone (photo, 2014).

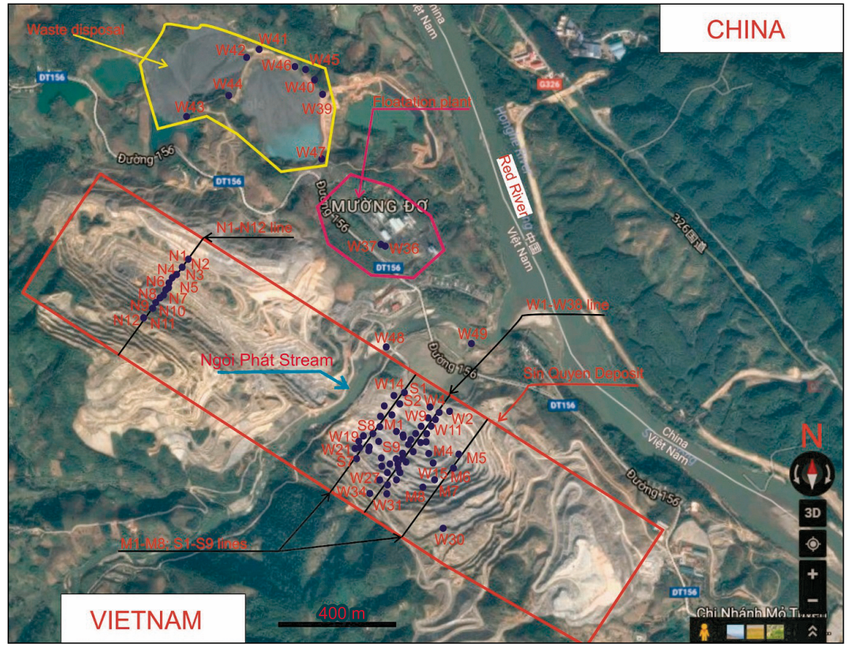

Fig. 6. Sampling localization.

sis, 39 samples were selected for analysis of the chemical compositions and natural radionuclides. The chemical composition was analyzed at Bureau Veritas Mineral Laboratories in Canada using the method assigned as AQ251 and NAA. The sample of 0.5 g was digested in Aqua Regia at 90 °C, and then ICP MS studies were carried out. A detailed description of the analytical methods, detection limits, and uncertainties can be downloaded from the ACME Laboratories website at www.acmelab.com. Analytical uncertainties are typically 5% for most of the analyzed elements. The detection limit for REE varies from 0.02 to 0.5 ppm. For the natural radionuclide determination, the sample was milled until the grains became smaller than 2 mm. Then it was dried in an oven at 120 °C for 24 h to ensure that moisture was completely removed. After that it was weighted and packed in a cylindrical aluminum beaker and sealed to prevent the escape of radon. The weighed and tightly sealed samples were left for at least 21 days to reach secular equilibrium between ^{226}Ra and ^{222}Rn as well as its "daughters" (mostly ^{214}Bi and ^{214}Pb). The activity concentration was determined using a semiconductor HPGe detector (Canberra GX4020) with 42% relative efficiency. The energy resolution of the spectrometer at the line 1333 keV (^{60}Co) is about 2 keV. As standard samples, reference materials RG produced by the International Atomic Energy Agency (IAEA) were used. Samples were measured in a cylindrical beaker with a volume of 48 cm^3 (sample diameter 70 mm, height 12.5 mm) placed directly on the detector. The sample measurement time amounted to about 50 h. A detailed description of the methodology is presented by Jodłowski and Kalita (2010).

RESULTS AND DISCUSSION

The analyzed chemical concentrations of most of the measured elements in the samples varied in the broad ranges (Table 1). The ratio of the maximum to minimum concentrations in the ore samples of the major elements ranges from 10^2 to 10^5 (ppm). The Fe concentration in the ore ranges from about 1 to 40%. The maximum concentration of Fe in the massive ore is at the level of that in the Fe concentrate (samples W18 and W37); Cu content ranges from about 0.004% to 11% (samples W31a and S4); the average Au and Ag concentrations are higher than those in the Earth's crust by about 10^5 and 10^3 times and equal to 1662 and 1163 ppb, respectively. Gold and silver are randomly occurring as an electrum mineral in vein forms (Fig. 7*a*). The economic or anomalous gold is characteristic of IOCG deposits in the world (Zhu, 2016). In the deposit the REE-bearing minerals are allanites occurring in a disseminated manner (Fig. 7*b*). The total concentration of rare-earth elements (TREE) var-

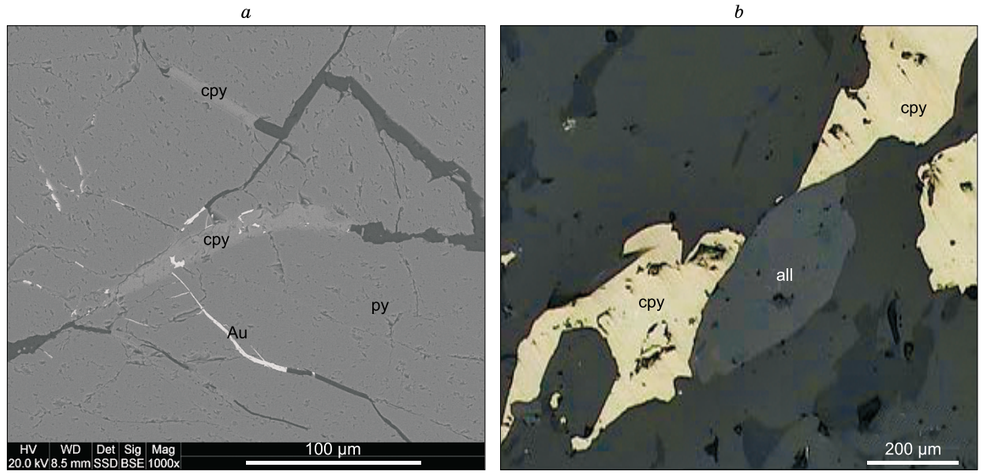

Fig. 7. BSE image showing the position of electrum (Au) in relation to pyrite (py) and chalcopyrite (cpy) (*a*); *b*, intergrowth of allanite (all) with chalcopyrite (cpy). Reflected light.

ies from 22 to about 2500 ppm with 700 ppm of average. The concentration of LREE is significantly higher than that of HREE, their average ratio (LREE/HREE) being equal to 70. The sulfur grade ranges from 0.06 to 7.5% with 2.04% of average. This value is about 10^3 times higher than the crustal average. The average U and Th concentrations are 84 and 13 ppm and higher than the Earth's average concentration by 24 and 1.4 times, respectively, so the uranium is the main radioactive element in the deposit. The general reasons for uranium enrichment in an IOCG deposit might include the hydrothermal fluids (Hitzman and Valenta, 2005).

Using the data in Table 1, the correlations between different elements were made, and their coefficients are summarized in Table 2. All the values of correlation coefficients (R) higher than 0.5 are marked in bold. According to the statistics background and excluding the relations between sulfur and iron with other elements, we consider only the strong relations, i.e., those with R higher than 0.7. The correlation coefficients between Cu and Ag, Te, Bi, Pb, and Au are higher than 0.7 and equal to 0.94, 0.94, 0.90, 0.82, and 0.73, respectively (Table 2, Fig. 8*a–e*). Copper, gold, and silver belong to the chalcophile elements group, which naturally prefers to bond with sulfur to form the resist compounds (Gas'kov, 2017; Palyanova et al., 2018). Gold and silver often occur together with pyrite, chalcopyrite, and pyrrhotite (Fig. 7*a*). These elements are in a strong correlation (R = 0.79 (Fig. 9)), indicating close similarity in their geochemical properties.

The Au–Ag alloy often occurs in microvein form in gold and copper minerals with trace elements of Hg (Gas'kov et al., 2001; Knight and Leitch, 2001). The Cu–Au correlation is lower than Cu–Ag (compare Figs. 8*a* and 8*e*), indicating that a part of Au formed separately in native form, and the other part of Au crystallized together with Ag and Cu. At the same time, silver is more affine to sulfur than to gold and tends to enter sulfide minerals (Gas'kov, 2017). These processes depend on the content of Au, Ag, and Cu in the hydrothermal fluid, crystallization temperature, and sulfur fugacity (Gas'kov, 2017; Palyanova et al., 2018). The significantly high concentrations of Au (>10,000 ppb) and Ag (>4000 ppb) are observed only in the samples of the massive Cu–Fe ore, suggesting electrum intergrowth with sulfide minerals, mainly in breccia ores. The high correlation coefficients are observed also for Cu–Te (R = 0.94) and Cu–Bi (0.90) (Table 2, Fig. 8*b*, *c*). In intrusive fluid high tellurium content can bind silver and gold and forms silver and gold tellurides (Gas'kov, 2017). In the Sin Quyen copper deposit, Te and Bi are trace elements with 1.9 and 1.4 ppm of average concentration, respectively. These concentrations are comparable with those in other IOCG deposits in the world (Mikulski, 2014). Generally the presence of Te and Bi in an IOCG deposit is related to the Au–Ag–Bi–Te–Pb mineral association as arsenopyrite and polymetallic sulfite (Mikulski, 2014). In the deposit, an intergrowth of bismuthinite (Bi_2S_3) with chalcopyrite (Fig. 10) indicates that these minerals crystallized at the similar temperature.

In the weathered zone, bismuthinite reacts with water and transforms into bismite (Bi_2O_3) or bismutite $Bi_2(CO_3)O_2$ (Gruszczyk, 1984). Figure 8*d* presents the relation between Cu and Pb with R = 0.82; Pb also belongs to chalcophile elements. The Pb, Te, and Bi concentrations are about several ppm (Table 1); therefore the elements in the IOCG deposits are regarded as the impurity rather than coproduct elements (Barton, 2014).

Table 1. Bulk chemical analyses of the samples from the Sin Quyen deposit (ACME Laboratories)

	Fe	Mn	Co	Ni	Au	Cu	Zn	Ag	Pb	Ga	Ge	S	Notes
Units	%	ppm	ppm	ppm	ppb	ppm	ppm	ppb	ppm	ppm	ppm	%	
MDL	0.01	1	0.1	0.1	0.2	0.01	0.1	2	0.01	0.1	0.1	0.02	
M1	25.52	274	328.7	240.3	502.6	11,539	40.9	508	2.79	4	0.3	7.46	Ep–Am rock, Cu–Fe ore
M2	7.74	308	47.6	21.4	511.1	32,225	85.9	1188	3.79	5.5	0.4	2.38	Ep–Am rock, Cu ore
M3	18.34	512	225.3	220.7	107.6	6751	21.6	216	4.98	5.1	0.7	3.97	Ep–Am rock
M4	29.14	226	119.7	43.4	991.8	44,900	67.9	1344	7.01	11.4	0.6	5.35	massive Cu–Fe ore
M5	28.45	528	82.3	22.7	343.5	29,700	50.3	1075	17.53	17.8	0.8	1.14	Cu–Fe ore
M6	13.36	499	57.2	27.4	237.5	26,524	187.1	711	5.29	10.7	0.5	1.69	Bt–Am rock, Cu ore
M7	31.35	305	71.8	37	59.3	4972	38.8	211	2.49	14.7	0.9	1.87	massive Fe ore
M8	24.28	1028	123	58.5	138	10,914	137.8	506	3.7	22.1	0.7	2.58	massive Cu–Fe ore
N1	4.31	330	24.1	18.7	657.3	8811	33.3	1034	1.64	10.7	0.4	0.91	Ep–Qtz–Pl rock
N2	1.18	137	4.5	10.3	102.3	404	9.1	98	1.5	4	0.1	0.06	Carbonate–quartz rock
N3	12.26	791	74.5	43.6	132.3	7695	48.4	754	2.38	22.9	0.7	2.15	skarn
N4	13.21	583	57.3	23.1	1204.4	16,976	173.5	1475	3.77	15.9	0.6	2.52	Bt–Am rock, Cu ore
N5	25.62	605	78.8	35.4	462.9	37,861	118.2	1569	3.13	16.4	0.7	1.85	Bt–Ep rock, Cu–Fe ore
N6	25.97	332	140.4	57.1	12,687.5	74,400	195.9	4159	33.92	13.8	0.6	2.66	Cu–Fe ore
N7	7.66	414	44.8	23.9	727.7	17,769	48.4	581	1.94	10.6	0.4	1.14	Cb–Qtz rock, Cu ore
N8	11.13	399	67.2	40.9	161.9	20,614	59.1	488	3.41	15	0.3	1.12	Bt–Qtz–Am rock Cu ore
N9	6.43	627	16.8	9.7	88.9	1302	26.4	83	1.31	9.1	0.4	0.16	Amphibolite
N10	12.89	449	86.9	35.2	175.9	28,309	96.4	952	2.8	23.1	0.3	1.26	Amphibolite Cu ore
N11	14.17	417	151.2	94.7	18,503.7	82,400	145.8	3050	24.27	11.7	0.3	2.95	Massive Cu ore
N12	20.72	332	41.2	18.5	598.1	11,258	51.8	498	3.84	15.5	0.5	0.86	Ep–Am rock, Cu–Fe ore
S1	10.21	521	61.2	45.6	121.2	3447	91.6	283	3.07	13.5	0.4	2.22	Bt–Am schist
S2	21.55	240	128.6	32	407.8	21,709	82.6	1668	3.56	15.9	0.7	2.23	Cu–Fe ore
S3	31.55	255	140.5	39.4	294.7	51,806	182.2	2311	26.21	13.4	0.7	2.02	Massive Cu–Fe ore
S4	30.6	114	182.2	91.3	10,531.2	107,878	152.2	4646	24.6	9.7	0.6	2.2	Massive Cu–Fe ore
S5	21.02	272	60	24	681.2	26150	77.9	1090	6.09	9.6	0.5	1.84	Cu–Fe ore
S6	21.53	244	139.9	51.7	2038.6	76,083	109.9	2939	15.53	7.7	0.5	2.43	Massive Cu–Fe ore
S7	2.08	156	3.6	4.9	10.4	394	12.6	30	0.89	6.2	0.1	0.07	Carbonate–quartz rock
S8	26.06	334	65.2	28.6	750.1	19,988	43.8	1844	2.14	18.6	0.7	1.75	Massive Cu–Fe ore
S9	23.59	173	112.1	41	897.7	58,040	104	2107	10.56	8.1	0.4	2.05	Cu–Fe ore
W-15	2.73	1085	12.2	7.3	3.1	186	32.5	8	1.76	–	–	0.1	ore, open pit
W-18	>40	319	99.2	41.4	2358.2	>10,000	88.3	1836	5.46	–	–	4.19	massive ore
W-25	5.81	758	66.1	35.7	28.6	2935	34.1	139	7.61	–	–	1.7	Ep–Am rock
W-31	15.28	1479	29.1	9.4	16.9	3067	57.7	113	3.11	–	–	0.41	skarn
W-31a	0.86	1264	2.3	<0.1	1.6	39	33.3	14	3.7	–	–	<0.02	skarn with garnet
Min	0.86	114	2.3	4.9	1.6	39	9.1	8	0.89	4	0.1	0.06	
Max	40	1479	328.7	240.3	18,504	107,900	196	4646	33.92	23.1	0.9	7.46	
Average	17.2	480	86.6	46.5	1662.81	25,670	80.6	1163	7.23	12.5	0.51	2.04	
Std. Dev	10.4	324	68.2	51.7	4033.42	27,465	53.45	1168	8.37	5.38	0.20	1.53	
W-36	35.0	236	183	91.6	6489.7	>10,000	580.1	30,909	40.8	–	–	8.33	Cu-concentrate
W-37	>40	356	135.3	84.8	148.2	998	28	230	3.56	–	–	3.62	Fe-concentrate
W-39	10.6	880	46.6	26.2	68.8	555	64.3	136	4.97	–	–	0.66	Waste I
W-40	9.57	792	36.6	24.1	67.3	386	52.2	86	4.2	–	–	0.6	Waste II
W-44	12.17	711	30.9	20.1	166.7	335	42.3	86	5.31	–	–	0.77	Waste out from tailing

Table 1. Continued

Elements	Sn	Te	Tl	Bi	Cd	U	Th	Sr	V	Cs	Cr	Ti	Notes
Units	ppm	ppm	ppm	ppm	ppm	ppm	ppm	ppm	ppm	ppm	ppm	%	
MDL	0.1	0.02	0.02	0.02	0.01	0.1	0.1	0.5	2	0.5	0.5	0.001	
M1	17.8	1.53	0.06	0.98	0.18	27.9	11.3	8.5	28	0.22	16	0.025	Ep–Am rock, Cu–Fe ore
M2	25.3	1.5	0.06	1.47	0.39	91.9	30.5	48	50	0.38	8.1	0.078	Ep–Am rock, Cu ore
M3	67.3	1.52	0.02	1.23	0.1	83.5	28.6	20.9	44	0.8	18.8	0.072	Ep–Am rock
M4	19.6	3.53	0.21	2.85	0.45	28.4	7.6	11.3	90	3.34	19.3	0.083	massive Cu–Fe ore
M5	14.8	1.71	0.57	1.22	0.23	219.7	12.6	102.1	104	6.72	20	0.141	Cu–Fe ore
M6	22.7	1.06	0.34	0.5	0.7	36.1	12.6	19.3	50	3.14	26.8	0.098	Bt–Am rock, Cu ore
M7	21.1	1.15	0.03	0.28	0.12	5	3.7	12.3	37	0.41	5	0.017	massive Fe ore
M8	17.1	2.42	0.18	0.8	0.32	5.9	5.7	32.2	69	5.5	9.6	0.058	massive Cu–Fe ore
N1	17.7	0.63	0.56	1	0.12	14.5	31.5	13.2	41	10.85	23.4	0.254	Ep–Qtz–Pl rock
N2	3.5	0.02	0.12	0.04	0.03	5.5	6.5	17	10	2.38	12.6	0.069	Carbonate–quartz rock
N3	18.1	1.04	1.28	1.4	0.1	53.9	19.2	26.8	99	26.32	50.3	0.241	skarn
N4	27.1	1.99	0.87	1.16	1.46	33.7	23.4	9.7	65	16.93	36.7	0.148	Bt–Am rock, Cu ore
N5	21.3	2.57	0.72	2.14	0.68	9.1	9.9	16.3	112	5.58	30	0.191	Bt–Ep rock, Cu–Fe ore
N6	37.9	5.52	0.46	3.81	1.58	514.7	11.8	27.7	103	2.6	20	0.113	Cu–Fe ore
N7	20.2	0.87	0.23	0.73	0.25	12.3	5.2	16.4	87	3.03	26.9	0.116	Cb–Qtz rock, Cu ore
N8	8.8	0.62	0.62	0.36	0.26	60.6	7.4	6.6	67	8	117	0.167	Bt–Qtz–Am rock Cu ore
N9	21.6	0.08	0.07	0.05	0.06	10.7	25.9	20.6	50	1.36	18.6	0.087	Amphibolite
N10	9.3	1.36	1.1	1.44	0.49	60.2	22.2	5.7	104	21.27	46.2	0.266	Amphibolite Cu ore
N11	20.8	4.44	0.42	4.64	1.02	335.6	10.1	17.8	78	2.27	32.5	0.061	Massive Cu ore
N12	5.6	1.14	0.88	0.84	0.15	41.6	14.3	8.3	87	14.41	63.8	0.266	Ep–Am rock, Cu–Fe ore
S1	18.5	0.66	1.88	0.73	0.21	50.8	9.1	8.5	48	48.69	25.7	0.199	Bt–Am schist
S2	10.4	1.32	0.72	2.36	0.72	30.3	13	17.7	92	11.22	4	0.116	Cu–Fe ore
S3	36.3	4.18	0.38	3.01	1.17	362.8	3	8.7	92	6.52	11.6	0.099	Massive Cu–Fe ore
S4	24.1	7.13	0.08	4.67	0.7	319.2	13.1	25	81	1.01	1.9	0.045	Massive Cu–Fe ore
S5	14	1.54	0.21	1.16	0.38	74.6	19.6	22.2	73	3.61	28.4	0.111	Cu–Fe ore
S6	18.5	3.95	0.22	2.31	0.57	139	22.5	43.7	67	1.51	15.8	0.074	Massive Cu–Fe ore
S7	1	0.03	0.06	0.06	0.01	3.3	12.8	6.7	15	0.63	6.9	0.015	Carbonate–quartz rock
S8	10.7	1.41	0.53	2.34	0.11	37.4	42.4	16.2	138	5.71	25.9	0.17	Massive Cu–Fe ore
S9	13.9	3.5	0.19	2.06	0.67	105	20.6	21.4	61	2.32	19.1	0.077	Cu–Fe ore
W-15	–	0.05	–	0.07	0.06	1.17	2.2	90.8	51	–	–	0.283	ore, open pit
W-18	–	3.6	–	2.58	0.41	56.51	2.9	11.4	123	–	–	0.075	massive ore
W-25	–	0.28	–	0.31	0.11	8.35	1.4	128	50	–	–	0.303	Ep–Am rock
W-31	–	0.15	–	0.56	0.03	16.31	0.9	22.3	74	–	–	0.268	skarn
W-31a	–	<0.02	–	0.08	0.07	0.98	0.5	98.2	<2	–	–	0.012	skarn with garnet
Min	1	0.02	0.02	0.04	0.01	0.98	0.5	5.7	10	0.22	1.9	0.012	
Max	67.3	7.13	1.88	4.67	1.58	514.7	42.4	128	138	48.69	117	0.303	
Average	19.5	1.9	0.5	1.4	0.4	84.0	13.6	28.3	70.9	7.5	25.5	0.1	
Std Dev.	12.4	1.7	0.4	1.3	0.4	122.6	10.2	30.3	30.2	10.3	22.5	0.1	
W-36	–	4.91	–	5.39	3.31	20.56	2.2	52.1	62	–	–	0.06	Cu-concentrate
W-37	–	0.64	–	1.28	0.1	22.7	2.9	13.1	219	–	–	0.125	Fe-concentrate
W-39	–	1.04	–	1.74	0.14	32.56	12.2	51	89	–	–	0.245	Waste I
W-40	–	0.86	–	1.32	0.14	30.64	8.7	45.1	83	–	–	0.256	Waste II
W-44	–	0.38	–	1.68	0.06	62.43	11.3	46	85	–	–	0.225	Waste out from tailing

Table 1. Continued

Elements	Ba	Mg	Al	Na	K	Ca	Nb	Rb	Sc	Y	LREE	HREE	TREE	Notes
Units	ppm	%	%	%	%	%	ppm	ppm	ppm	ppm	ppm	ppm	ppm	
MDL	0.5	0.01	0.01	0	0.01	0.01	0.02	0.01	0.02	0.01	0.01	0.01	0.01	
M1	7	0.14	0.55	0.09	0.14	1.09	0.74	2.5	1.1	6.65	487	3.8	490	Ep–Am rock, Cu–Fe ore
M2	6.7	0.34	0.95	0.12	0.19	2.16	1.5	4.9	3.2	20.41	2245	11.1	2256	Ep–Am rock, Cu ore
M3	4	0.03	0.59	0.01	0.02	4.12	2.49	3.8	1.8	81.39	1077	44.4	1122	Ep–Am rock
M4	13.4	0.25	0.56	0.06	0.25	0.59	2.55	24.5	2	9.49	704	4.7	709	massive Cu–Fe ore
M5	170	1.71	2.03	0.02	2.3	2.58	2.03	115	3.3	17.2	1378	10.3	1388	Cu–Fe ore
M6	130	0.53	1.63	0.08	1.15	1.4	1.27	56.8	2.6	9.12	622	5.1	627	Bt–Am rock, Cu ore
M7	10.9	0.14	0.68	0.11	0.13	0.92	0.33	4.3	1.4	4.24	145	2.3	148	massive Fe ore
M8	88.2	0.69	2.13	0.11	0.48	2.37	0.28	58.2	3.7	8.32	214	4.8	219	massive Cu–Fe ore
N1	197	2.77	2.82	0.07	2.81	0.57	0.26	112	7.5	46.83	1466	25.9	1492	Ep–Qtz–Pl rock
N2	53.8	0.61	0.88	0.16	0.58	1.51	0.26	24.4	3.7	38.6	575	19.7	595	Carbonate–quartz rock
N3	247	3.39	4.81	0.01	3.87	1.99	1.2	194.2	5.5	11.97	961	6.0	967	skarn
N4	128	0.59	2.16	0.17	1.11	1.29	1.14	107.7	6.2	14.87	672	7.8	680	Bt–Am rock, Cu ore
N5	155	1.52	2.28	0.03	2.21	1.04	1.47	114.4	11.9	13.33	832	7.2	840	Bt–Ep rock, Cu–Fe ore
N6	80.6	0.48	1.08	0.04	0.62	1.02	0.72	39.1	2.4	17.85	626	10.2	636	Cu–Fe ore
N7	112	0.91	1.99	0.2	0.76	1.46	0.37	37.8	3.4	9.57	184	4.8	189	Cb–Qtz rock, Cu ore
N8	241	2.64	3.79	0.05	2.55	0.3	0.34	112	6.1	7.43	126	4.1	130	Bt–Qtz–Am rock, Cu ore
N9	21.3	1.26	2.16	0.34	0.26	2.82	0.27	10.3	4.1	13.91	173	6.8	179	Amphibolite
N10	284	5.43	5.9	0.01	4.11	0.32	1.11	178.5	5.7	8.2	154	4.5	159	Amphibolite Cu ore
N11	34.2	1.5	2.42	0.07	0.3	1.51	0.43	20.4	2.5	10.17	292	6.1	298	Massive Cu ore
N12	364	1.12	3.22	0.05	2.97	0.38	0.98	150	3.6	7.09	475	3.3	478	Ep–Am rock, Cu–Fe ore
S1	159	3.35	3.57	0.03	3.3	0.46	0.58	294.2	2.4	4.99	421	2.5	424	Bt–Am schist
S2	104	2.57	2.19	0.03	2.84	0.49	1.73	170	2.2	10.4	656	4.9	661	Cu–Fe ore
S3	57.6	0.5	1	0.04	0.79	0.6	1.55	59	1.6	11.42	177	6.4	184	Massive Cu–Fe ore
S4	12.9	0.25	0.3	0.02	0.17	0.98	1.41	9.4	1.1	30.56	1694	15.8	1710	Massive Cu–Fe ore
S5	74.8	0.45	1.14	0.1	0.72	0.76	1.95	45	3.5	9.55	1316	5.2	1321	Cu–Fe ore
S6	32.4	0.46	0.93	0.11	0.43	1.56	1.5	24.7	2.8	17.35	2455	8.9	2464	Massive Cu–Fe ore
S7	20	0.29	0.79	0.05	0.2	0.49	0.08	14.9	2.1	14.18	167	6.7	173	Carbonate–quartz rock
S8	170	0.68	1.8	0.04	1.38	0.65	0.71	88.4	3.5	11.06	1364	5.6	1369	Massive Cu–Fe ore
S9	48.3	0.34	0.81	0.08	0.51	0.64	1.59	30.8	1.8	10.18	1236	5.3	1241	Cu–Fe ore
W-15	154	1.03	8.52	4.22	1.34	6.72	–	–	9	17	51	7.3	59	ore, open pit
W-18	12.8	0.55	1.5	0.56	0.22	0.55	–	–	5	10	239	3.6	242	massive ore
W-25	18.1	1.6	6.21	1.22	0.29	3.23	–	–	22	66	189	24.6	213	Ep–Am rock
W-31	31.4	3.61	4.58	1.03	1.07	6.04	–	–	16	52	122	20.7	142	skarn
W-31a	6.2	0.26	1.95	0.02	0.02	29.1	–	–	1	11	19	2.4	22	skarn with garnet
Min	4	0.03	0.3	0.01	0.02	0.3	0.08	2.5	1	4.24	19	2	22	
Max	364	5.43	8.52	4.22	4.11	29.1	2.55	294.2	22	81.39	2455	44	2464	
Average	95.6	1.2	2.3	0.3	1.2	2.4	1.1	72.7	4.6	18.6	692	9	701	
Std Dev.	92.4	1.3	1.9	0.7	1.2	5.0	0.7	71.7	4.4	17.9	632	9	634	
W-36	36.1	0.32	1.07	0.24	0.29	1.9	–	–	5	17	542	4.5	546	Cu-concentrate
W-37	36.5	0.42	1.35	0.42	0.37	0.53	–	–	3	15	920	4.5	925	Fe-concentrate
W-39	204	1.94	6.41	1.88	2.17	3	–	–	13	49	2550	18.9	2569	Waste I
W-40	189	1.85	6.23	1.88	2.01	2.7	–	–	13	55	2559	15.8	2575	Waste II
W-44	104	1.39	5.52	1.59	1.15	2.79	–	–	13	99	5450	21	5471	Waste out from tailing

Table 2. Correlation coefficients for ore and impurity elements in the samples from the Sin Quyen deposit

Elements	Cu	Fe	Mn	Co	Ni	Au	Zn	Ag	Pb	Ga	Ge	S	Sn	Te	Tl	Bi	Cd	U	Th	V	REE
Cu	1																				
Fe	**0.53**	1																			
Mn	–0.44	0.1	1																		
Co	0.46	**0.59**	–0.08	1																	
Ni	0.15	0.31	0.05	**0.9**	1																
Au	**0.73**	0.17	–0.12	0.33	0.21	1															
Zn	**0.67**	0.39	–0.09	0.26	–0.04	0.49	1														
Ag	**0.94**	**0.5**	–0.22	0.41	0.11	**0.74**	**0.68**	1													
Pb	**0.82**	0.46	0.22	0.41	0.16	**0.74**	**0.64**	**0.82**	1												
Ga	–0.08	0.28	**0.59**	–0.17	–0.32	–0.05	0.23	0.03	–0.03	1											
Ge	0.11	–0.18	0.33	0.21	0.05	–0.07	0.24	0.21	0.2	0.49	1										
S	0.26	0.2	0.02	**0.83**	**0.77**	0.18	0.2	0.25	0.16	–0.18	0.18	1									
Sn	0.19	0.28	0.18	0.47	**0.55**	0.19	0.29	0.22	0.36	–0.19	0.42	0.39	1								
Te	**0.94**	0.35	–0.22	**0.56**	0.26	**0.69**	**0.7**	**0.93**	**0.82**	0.01	0.29	0.42	0.34	1							
Tl	–0.18	–0.32	0.35	–0.22	–0.22	–0.09	0.13	–0.08	–0.13	**0.61**	0.07	0.14	–0.18	–0.18	1						
Bi	**0.90**	0.14	–0.26	**0.51**	0.23	**0.76**	**0.6**	**0.92**	**0.77**	0.08	0.25	0.4	0.28	**0.91**	**0.53**	1					
Cd	**0.67**	–0.19	–0.05	0.29	0.03	**0.56**	**0.89**	**0.73**	**0.69**	0.13	0.2	0.23	0.33	**0.69**	0.08	**0.66**	1				
U	**0.78**	0.41	–0.23	0.35	0.11	**0.78**	**0.62**	**0.81**	**0.97**	0.03	0.14	0.09	0.31	**0.78**	–0.04	**0.75**	**0.69**	1			
Th	0.08	0.14	–0.35	–0.15	–0.18	–0.03	–0.14	0.18	–0.03	–0.14	–0.24	–0.2	–0.3	0.04	–0.08	0.09	–0.04	–0.03	1		
V	0.39	**0.56**	0.2	0.08	–0.17	0.21	0.34	0.47	0.3	**0.69**	**0.53**	0.1	0.03	0.43	0.46	**0.56**	0.33	0.33	0.03	1	
REE	0.46	0.26	–0.41	0.20	0.08	0.08	0.12	0.48	0.21	–0.27	0.16	0.17	0.14	0.36	–0.17	0.37	0.11	0.21	**0.64**	0.13	1

Generally uranium and thorium minerals, such as uraninite, thorite, thorianite, and allanite, are often present in IOCG deposits. Although low-grade enough, the world's greatest uranium resource is in the IOCG Olympic Dam deposit in Australia (9.2 Gt at 270 ppm U); the smaller uranium resources occur in other IOCG assemblages, including the Kangdian metallogenic province in SW China, the Qiaoxiahala deposit in the Jungar region, NW China, the Ayazmant skarn deposit in Ayvalık (Balıkesir), Turkey, and others (Hitzman and Valenta, 2005; Oyman, 2010; Li et al., 2014; Chen et al., 2015). The main uranium-bearing mineral in the Sin Quyen deposit is uraninite. This mineral often exists as an intergrowth with chalcopyrite, magnetite, and allanite in the massive Cu–Fe ore (Fig. 11). Owing to the high uranium concentration, the Sin Quyen deposit was discovered by radiometric survey (Ta, 1975). The correlation coefficient of the Cu–U amounts to 0.78 (Table 2). A similar correlation coefficient of Cu–U was observed in the case of the Polish copper mines in the Lubin mining district (Niewodniczański, 1981; Piestrzyński, 1989).

Iron is the basic element in the studied deposit; its concentration varies from about 1 to above 40%. However, the coefficients of the correlation between this element and other elements were relatively low (≤0.6). The low correlation coefficients of Fe with other elements in the study deposit were also reported by Gas'kov et al. (2012). The weak correlation of Fe is probably connected with the geochemical property of this element. In nature Fe can occur in the oxidation state of 2+ or 3+ and rarely 0. Depending on the redox and chemical conditions, Fe can bond with sulfur or oxygen and form sulfate or sulfide or oxide compounds. In the Sin Quyen deposit, there are many Fe-bearing minerals, such as rock-forming chalcopyrite, bornite, pyrrhotite, pyrite, and magnetite, indicating that in the deposit there were inhomogeneous fluids. Several crystallization stages accompanied by different geologic and crystallization conditions were recognized in the deposit (Gas'kov et al., 2012; Pieczonka et al., 2015; Li and Zhou, 2018). Additionally there are some zones characterized by different major minerals (Gas'kov et al., 2012; Pieczonka et al., 2015). Using the archival data reported by Ta (1975), the plot of the relation between two principal elements Cu and Fe in the deposit is shown in Fig. 12.

The Cu–Fe plot (Fig. 12) can be divided into two parts. In the first part, there are relatively low concentrations of both Fe and Cu, and it is characterized by Fe content linearly increasing with an increase in Cu content. In the second part, Fe is dominating and decreasing with an increase in Cu content. The two mentioned parts might correspond to the two types of ores described by Gas'kov et al. (2012). The sam-

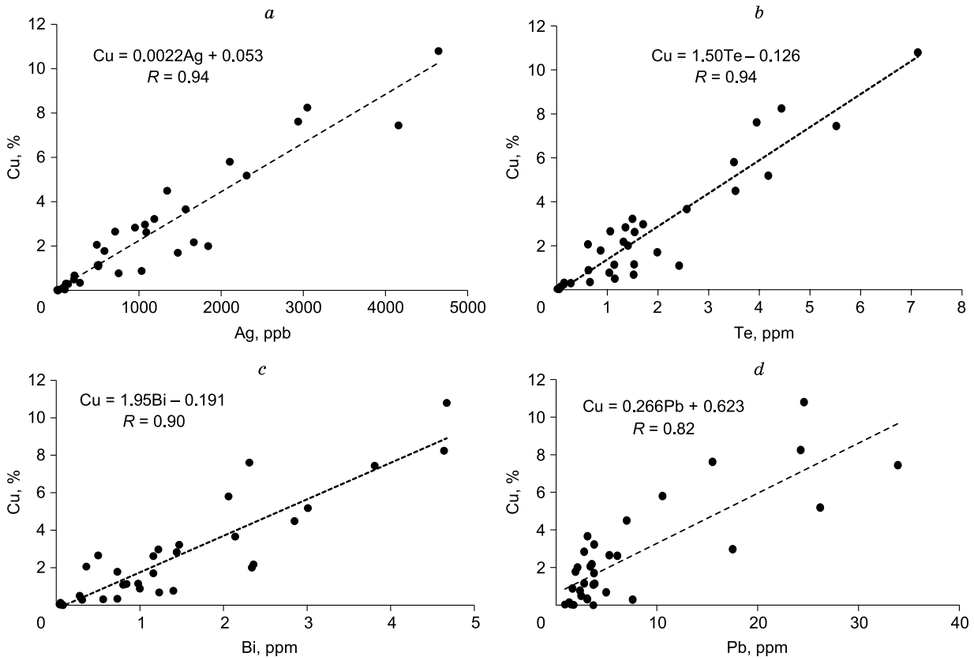

Fig. 8. Plots of the relations between Cu and Ag (*a*), Te (*b*), Bi (*c*), Pb (*d*), and Au (*e*).

Fig. 9. Plot of the relation between Au and Ag.

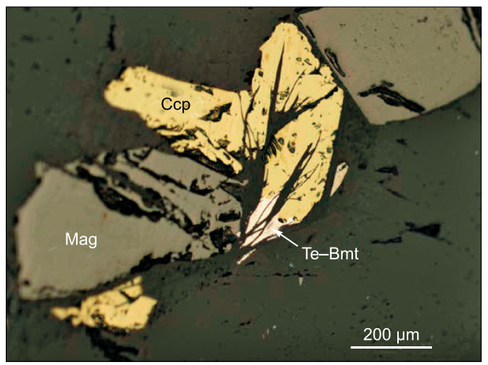

Fig. 10. Te-bismuthinite (Te-Bmt) with chalcopyrite (Ccp) in reflected light.

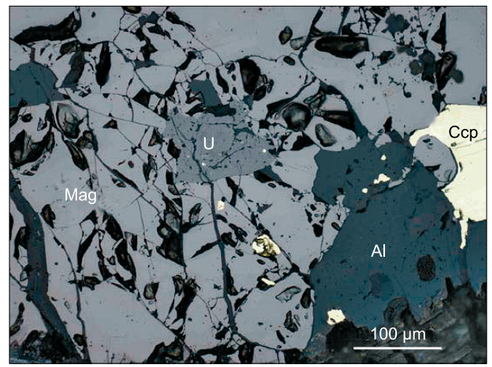

Fig. 11. Intergrowth of uraninite (U) with magnetite (Mag), chalcopyrite (Ccp), and allanite (Al), reflected light.

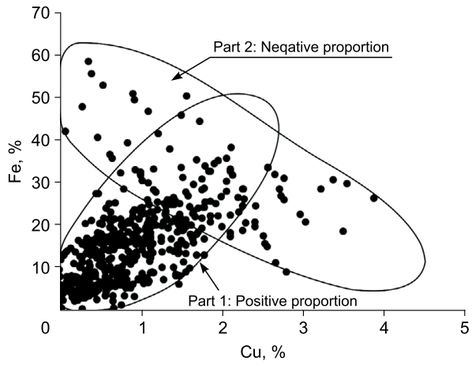

Fig. 12. Plot of the relation between Fe and Cu concentration, data from (Ta, 1975).

ples with positive correlation belong to the first zone, and most of the samples with negative correlation are within the second deposit part.

Cobalt and nickel are typical siderophile elements and often occur in the sulfoarsenides or with Fe in pyrrhotite or pyrite, but their grades in an IOCG deposit rarely exceed 100 ppm (Barton, 2014; Gas'kov, 2017). In the Sin Quyen deposit, the concentrations of these elements range from a few ppm to 300 ppm (Table 1). The maximum concentrations are far below the economic grade of a Co–Ni deposit. The correlation coefficient is equal to 0.9 (Table 2), and the view of the plot of the Ni–Co couple is shown in Fig. 13*a*. The high correlation coefficient reflects the close mineralogical association of Co and Ni and the comparable concentration ranges of these elements in the study deposit. The correlation coefficient of the Fe–Co pair amounts only to 0.62 (Fig. 13*b*), but the value of the correlation coefficient of the Co–S pair is equal to 0.83 (Table 2, Fig. 13*c*), suggesting that Co mostly occurs as a substitution at the sulfides.

Natural radioactive elements often play very important roles in the geophysical survey, especially for deposits rich in these elements. The average activity concentrations of

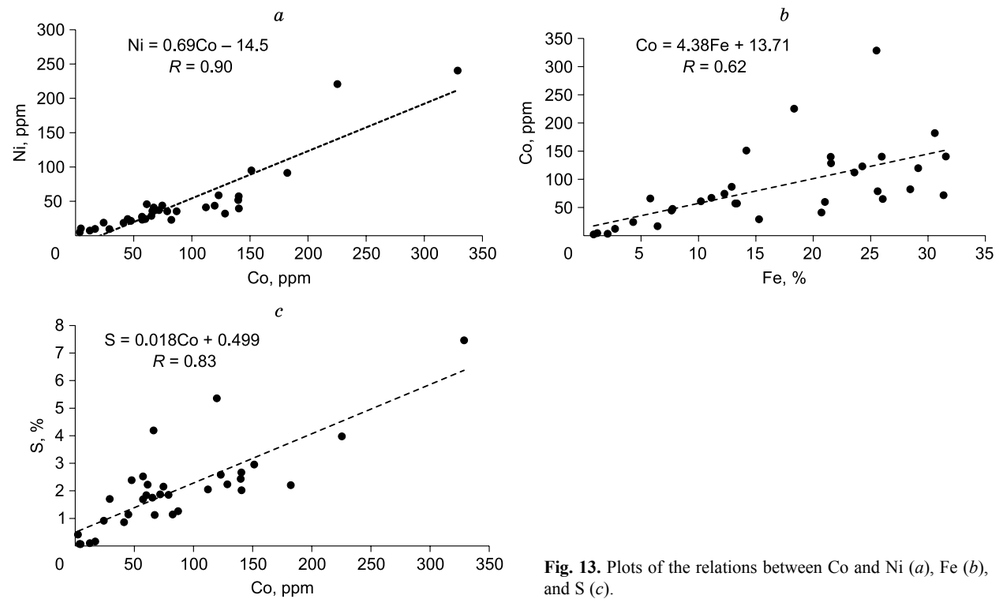

Fig. 13. Plots of the relations between Co and Ni (*a*), Fe (*b*), and S (*c*).

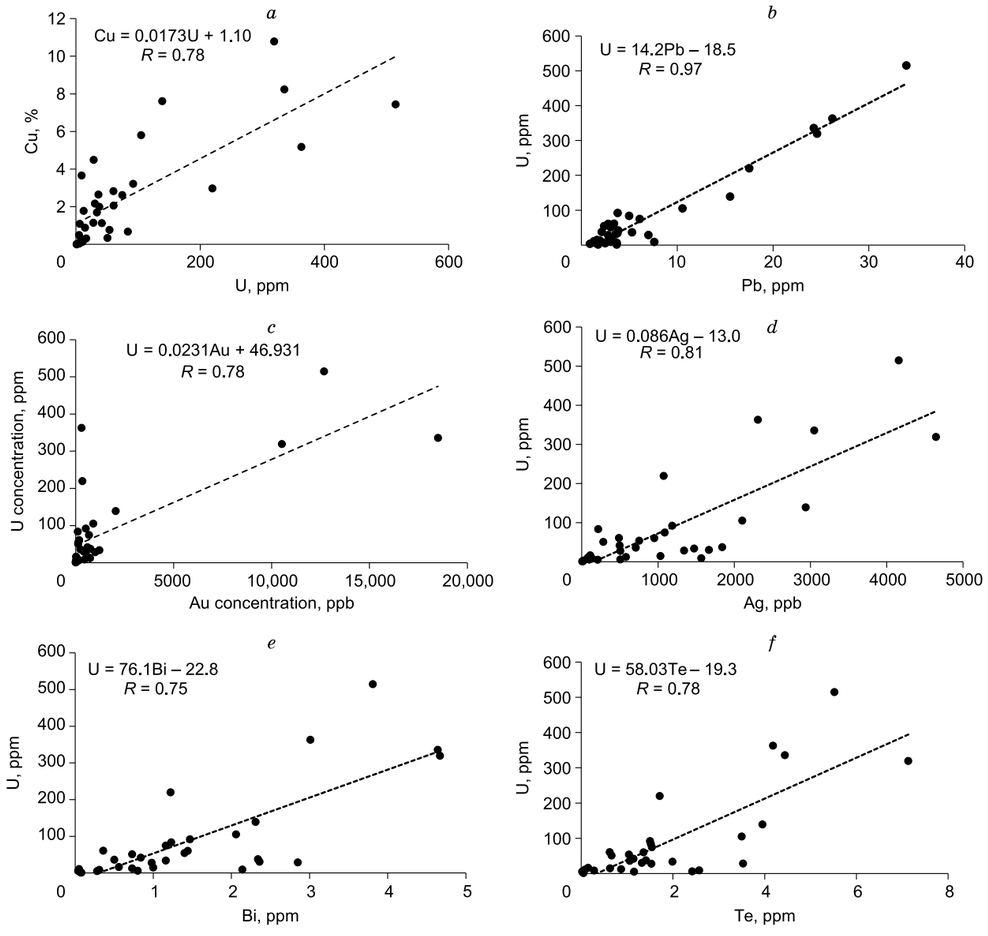

Fig. 14. Plots of the relations between U and Cu (*a*), Pb (*b*), Au (*c*), Ag (*d*), Bi (*e*), and Te (*f*).

^{40}K, ^{226}Ra, and ^{232}Th in the Sin Quyen deposit were recorded at 496, 691, and 59 Bq/kg, respectively. The correlation coefficients of the pairs U–Cu, U–Pb, U–Au, U–Ag, U–Bi, and U–Te amount to 0.78, 0.97, 0.78, 0.81, 0.75, and 0.78, respectively (Table 2, Fig. 14*a–f*). Such a high correlation enables us to determine the mentioned nonradioactive elements in the solid samples through measurements of uranium and to save the analysis costs significantly. In the Sin Quyen deposit, the principal radioactive element is uranium (Nguyen et al., 2016). The main uranium-bearing mineral is uraninite, which is often observed within the massive copper ores (Ishihara et al., 2011; Pieczonka et al., 2015). The high correlation coefficient of U–Pb (R = 0.97 (Fig. 14*b*)) is probably connected with the ^{206}Pb isotope (the last isotope in the uranium series), which principally contributes to the total lead content in the deposit. The good correlation between U and Au, Ag, Bi, and Te suggests that the minerals bearing these elements principally crystallized at the similar temperatures. According to Gas'kov (2008), the crystallization temperatures of the minerals bearing the mentioned elements (uraninite, tellurobismuthite, and sulfoaresenides) varied from 200 to 75 °C.

The reservoir of the REE is in the third place after Fe and Cu in the Sin Quyen deposit (Ta, 1975; McLean, 2001; Ishihara et al., 2011; Gas'kov et al., 2012; Li and Zhou, 2018). The main REE-bearing mineral is allanite (Fig. 11). Usually it occurs either at low concentrations, 1–2 vol.%, or very rarely as a major mineral. The average content of allanites in the ore is at the level of 0.98 wt.% (Pieczonka et al., 2015). There is no correlation with the other elements observed,

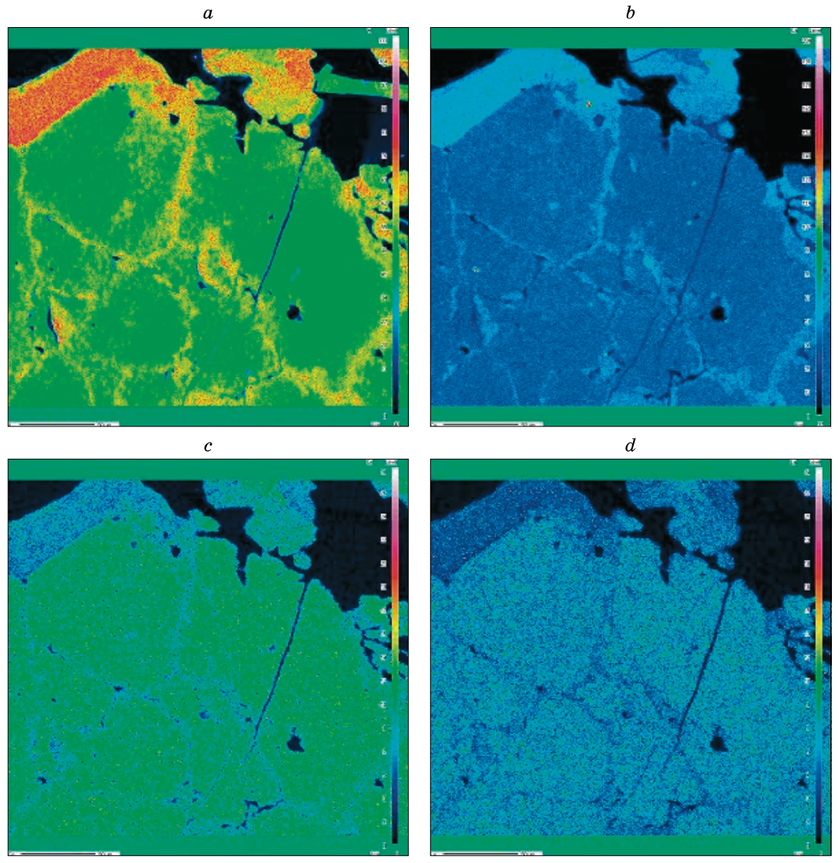

Fig. 15. Contour map of Al (*a*), Ca (*b*), Ce (*c*), La (*d*), Nd (*e*), and Ti (*f*) in allanites.

suggesting that allanites formed separately from the sulfide and oxide ores (Gas'kov et al., 2012).

In the deposit there are two groups of allanites (Fig. 15*a–d*); the outer rim is younger. Different tints in the gray color show mosaic textures of allanite crystals. This can be interpreted either as a change in the fluid composition during crystallization or as changes in the composition during Na-alteration (Li and Zhou, 2018). The older allanite group is with REE content from 23 to 27%, and the younger with 19 to 23% and higher amounts of Al_2O_3, CaO, and SiO_2 (McLean, 2001; Pieczonka et al., 2015). The allanites can be classified as La–Ce-ferriallanite and a variety with low Y, U, and Th. The difference between the mentioned two groups might result from the alteration processes occurring in the study deposit.

Sulfur is a very interesting element in an IOCG deposit; its average concentration in the deposit amounts to 2.04%

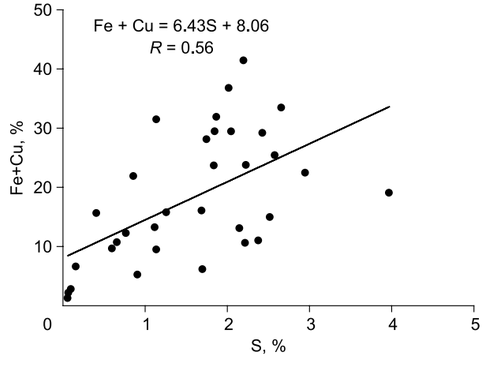

Fig. 16. Plot of relation between S and (Cu + Fe).

(Table 2). The sulfur minerals are dominating in the deposit, but, excluding the relation between S and Co, the correlation coefficients of the relation between sulfur and other major, minor, and trace elements are below 0.5 (Table 2). The relation between S and other elements is considered in this paper for the first time. In general, the crystallization of the sulfur minerals requires relatively oxidized ($SO_4^{2-} > H_2S$) sulfur low in total content (Barton, 2014). In an IOCG deposit, sulfur occurs in different sulfides (pyrite, chalcopyrite, and pyrrhotite). Owing to high chemical activity, sulfur is easily bound with different elements to form different minerals. Therefore the total sulfur is spread into many compounds, and there is no clear correlation between these elements and the others. The suggestion was tested by the correlation between sulfur and the sum of Fe and Cu (Fe + Cu), whose correlation coefficient R is equal to 0.56 (Fig. 16). The value is far higher than that of the correlation between Cu and other single elements.

CONCLUSIONS

Generally, the statistical analysis is very important in most practical matters. In Earth sciences the statistical calculus is named “geostatistics”, which consists in the probability and statistical correlation between different parameters of the geologic objects. The authors of this paper attempted to deal with the relations between the major, minor, and trace elements, focusing on the strong correlations and inspected relations. Based on the presented results and calculated correlation coefficients, as well as geological and geochemical analyses, we make the following conclusions:

(1) There are strong correlations between the elements of the chalcophile group (Cu, Ag, Au, Pb, Bi, and Te). The correlation coefficients between the elements in this group are higher than 0.7 and not sensitive to the ranges of the element concentrations;

(2) The correlation between Fe and other elements, even with Co and Ni, which belong to the siderophile group, is very weak or not observed. The phenomena might be a consequence of the chemical property of iron and geologic and geochemical conjunctures in the Sin Quyen IOCG deposit. It is worth adding that there is strong correlation between Co and Ni, because both elements not only have a close mineralogical association, but also their grade ranges are comparable in the deposit;

(3) Between Cu and Fe, there are clearly two relations: a positive relation and a negative relation. The two relations are probably connected with the two horizontally separated parts of the Sin Quyen deposit;

(4) There is a strong correlation between uranium and Cu, Ag, Au, Pb, Bi, and Te. The strong correlation between U and Cu, Ag, and Au might result from the crystallization of uraninite together with the chalcopyrite and electrum minerals in the deposit;

(5) There is a very weak, if any, correlation between REE and other elements, probably because allanite formed separately from the other minerals (Li et al., 2017);

(6) There is no correlation between sulfur and major and minor or trace elements because of the very high chemical activity of this element. Sulfur is sensitive to the crystallization (temperature and pressure) and redox conditions and easily reacts with many elements to form crystallized compounds. Therefore there is no strong correlation between sulfur and other single elements.

The work was made in the scope of the bilateral cooperation between the Hanoi University of Mining and Geology (UMG) and AGH University of Science and Technology No. 01/2012/HD-HTQTSP. The study was funded by UST-AGH Krakow, grants no. 11.11.140.161 and 11.11.140.645.

REFERENCES

Barton, M.D., 2014. 13.20 - Iron Oxide (–Cu–Au–REE–P–Ag–U–Co) Systems, in: Treatise on Geochemistry, 2nd ed. Elsevier, Vol. 13, pp. 515–541, doi: 10.1016/B978-0-08-095975-7.01123-2.

Bonev, I.K., Kerestedjian, T.K., Atanassova, R., Andrew, C.J., 2002. Morphogenesis and composition of native gold in the Chelopech volcanic-hosted Au-Cu epithermal deposit, Srednogorie zone, Bulgaria. Miner. Deposita 37, 614–629, doi: 10.1007/s00126-002-0273-8.

Chen, W.T., Zhou, M.F., Gao, J.-F., Hu, R., 2015. Geochemistry of magnetite from Proterozoic Fe-Cu deposits in the Kangdian metallogenic province, SW China. Miner. Deposita 50, 795–809, doi: 10.1007/s00126-014-0575-7.

Fabris, A., van der Wielen, S., Keeping, T., Gordon, G., 2015. Geochemical footprints of IOCG deposits beneath thick cover: insights from the Olympic Cu-Au province, South Australia. Conf. Materials of 27th Int. Appl. Geochem. Symp. (IAGS). Tucson, Ariz., pp. 20–24.

Gandhi, S.S., 2003. An overview of the Fe oxide-Cu-Au deposits and related deposit types. CIM Montreal 2003 Min. Ind. Conf. and Exhibition, Can. Inst. Min., Tech. Pap., CD-ROM.

Gas’kov, I.V., 2008. New data on the correlation of skarn and gold mineralization at the Tardan deposit (northeastern Tuva). Russ. Geol. Geophys. 49 (12), 923–931, doi: 10.1016/j.rgg.2008.01.011.

Gas’kov, I.V., 2017. Major impurity elements in native gold and their association with gold mineralization setting in deposits of Asian folded areas. Russ. Geol. Geophys. 58 (9), 1080–1092, doi: 10.1016/j.rgg.2017.08.004.

Gas’kov, I.V., Distanov, E.G., Kovalev, K.R., Akimtsev, V.A., 2001. Gold and silver in polymetallic deposits of northwestern Rudny Altai. Russ. Geol. Geophys. 42 (6), 850–867.

Gas’kov, I.V., Tran, T.A., Tran, T.H., Pham, T.D., Nevolko, P.A., Pham, N.C., 2012. The Sin Quyen Cu-Fe-Au-REE deposit (northern Vietnam) composition and formation conditions. Russ. Geol. Geophys. 53 (5), 442–456, doi: 10.1016/j.rgg.2012.03.005.

Groves, D.I., Bierlein, F.P., Meinert, L.D., Hitzman, M.W., 2010. Iron oxide copper-gold (IOCG) deposits through Earth history: Implications for origin, lithospheric setting, and distinction from other epigenetic iron oxide deposits. Econ. Geol. 105, 641–654, doi: 10.2113/gsecongeo.105.3.641.

Gruszczyk, H., 1984. Science of Ores [in Polish]. WG, Warsaw.

Hitzman, M.W., Valenta, R.K., 2005. Uranium in iron oxide-copper-gold (IOCG) systems. Econ. Geol. 100, 1657–1661, doi: 10.2113/gsecongeo.100.8.1657.

Hitzman, M.W., Oreskes, N., Einaudi, M.T., 1992. Geological characteristics and tectonic setting of Proterozoic iron oxide (Cu–U–Au-REE) deposit. Precambrian Res. 58, 241–287, doi: 10.1016/0301-9268(92)90121-4.

Ishihara, S., Hideo, H., Mihoko, N.C., Pham, T.D., Pham, T.A., Tran, T.H., 2011. Mineralogical and chemical characteristics of the allanite-rich copper and iron ores from the Sin Quyen mine, northern Vietnam. Bull. Geol. Surv. Japan 62 (5–6), 197–209.

Jodłowski, P., Kalita, S., 2010. Gamma-Ray Spectrometry Laboratory for high-precision measurements of radionuclide concentrations in environmental samples. Nukleonika 55 (2), 143−148.

Knight, J., Leitch, C.H.B., 2001. Phase relations in the system Au–Cu–Ag at low temperatures, based on natural assemblages. Can. Mineral. 39, 889–905, doi: 10.2113/gscanmin.39.3.889.

Letnikova, E.F., Veshcheva, S.V., Proshenkin, A.I., Kuznetsov, A.B., 2011. Neoproterozoic terrigenous deposits of the Tuva–Mongolian massif: geochemical correlation, source lands, and geodynamic reconstruction. Russ. Geol. Geophys. 52 (12), 1662–1671, doi: 10.1016/j.rgg.2011.11.013.

Li, Q., Zhang, Z., Geng, X., Li, C., Liu, F., Chai, F., Yang, F, 2014. Geology and geochemistry of the Qiaoxiahala Fe-Cu-Au deposit, Junggar region, northwest China. Ore Geol. Rev. 57, 462–481.

Li, X.C., Zhou, M.F., 2018. The nature and origin of hydrothermal REE mineralization in the Sin Quyen deposit, northwestern Vietnam. Econ. Geol. 113 (3), 645–673, doi: 10.5382/econgeo.2018.4565.

Li, X.C., Zhou, M.F., Chen, W.T., Zhao, X.F., Tran, M.D., 2017. Uranium-lead dating of hydrothermal zircon and monazite from the Sin Quyen Fe-Cu-REE-Au-(U) deposit, northwestern Vietnam. Miner. Deposita 53 (3), 399–416, doi: 10.1007/s00126-017-0746-4.

McLean, R.N., 2001. The Sin Quyen iron oxide–copper–gold–rare earth oxide mineralization of North Vietnam, in: Porter, T.M. (Ed.), Hydrothermal Iron Oxide Copper-Gold and Related Deposits: A Global Perspective. PGC Publ. 2, pp. 293–301.

Mikulski, S.Z., 2014. The occurrence of tellurium and bismuth in the gold-bearing polymetallic sulfide ores in the Sudetes (SW Poland). Miner. Resour. Manage. 30 (2), 15–34.

Nguyen, D.C., Le, K.P., Jodłowski, P., Pieczonka, J., Piestrzyński, A., Duong, H.V., Nowak, J., 2016. Natural radioactivity at the Sin Quyen iron oxide copper gold deposit in North Vietnam. Acta Geophys. 64 (6), 2305–2321.

Niewodniczański, J., 1981. A radiometric analysis of nonradioactive ores [in Polish with summary in English]. Sci. Bull. The Stanisław Staszic Acad. of Min. and Metall., No. 303 “Mathematics-Physics-Chemistry”. Krakow, Poland.

Nikiforova, Z.S., Gerasimov, B.B., Glushkova, E.G., Kazhenkina, A.G., 2018. Indicative features of placer gold for the prediction of the formation types of gold deposits (east of the Siberian Platform). Russ. Geol. Geophys. 59 (10), 1318–1329, doi: 10.1016/j.rgg.2018.09.009.

Oyman, T., 2010. Geochemistry, mineralogy and genesis of the Ayazmant Fe-Cu skarn deposit in Ayvalik, (Balikesir), Turkey. Ore Geol. Rev. 37, 175–201, doi: 10.1016/j.oregeorev.2010.03.002.

Palyanova, G.A., Murzin, V.V., Zhuravkova, T.V., Varlamov, D.A., 2018. Au-Cu-Ag mineralization in rodingites and nephritoids of the Agardag ultramafic massif (southern Tuva, Russia). Russ. Geol. Geophys. 59 (3), 238–256, doi: 10.1016/j.rgg.2018.03.003.

Pham, Q.D., 2015. Exploration report on no.3 and no.7 ore bodies of the Sin Quyen deposit, Lao Cai province. Archival Mag. of Natl. Geol. Dept. of Vietnam.

Pieczonka, J., Piestrzyński, A., Le, P.K., Nguyen, C.D., Jodłowski, P., 2015. Rare Earth, radioactive and selected elements in the iron oxide copper gold Sin Quyen deposit in North Vietnam, in: Viet-Pol 2015 Second Int. Conf. on Sci. Res. Cooperation between Vietnam and Poland in Earth Sciences, pp. 331–353.

Pieczonka, J., Nguyen, C.D., Piestrzyński, A., Le, P.K., 2019. Timing of ore mineralization using ore mineralogy and U-Pb dating in IOCG Sin Quyen deposit, North Vietnam. Geol. Q. 63 (4), 861–874.

Piestrzyński, A., 1989. Uranium and thorium in copper ore deposits on the Fore-Sudetic Monocline (SW Poland). Mineral. Pol. 20 (1), 41–53.

Requia, K., Fontboté, L., 2000. The Salobo iron-oxide copper-gold deposit, Carajás, northern Brazil, in: Porter, T.M. (Ed.), Hydrothermal Iron Oxide Copper-Gold and Related Deposits: A Global Perspective. PGC Publ., Adelaide, pp. 225–236.

Requia, K., Stein, H., Fontboté, L., Chiaradia, M., 2003. Re-Os and Pb-Pb geochronology of the Archean Salobo iron oxide copper-gold deposit, Carajas mineral province, northern Brazil. Miner. Deposita 38, 727–738.

Ta, V.D., 1975. Report of geological surveys and their results performed at the IOCG Sin Quyen deposit in Lao Cai, North Vietnam. Main Dept. of Geol. of Vietnam.

Zhao, X.F., Zhou, M.F., 2011. Fe–Cu deposits in the Kangdian region, SW China: a Proterozoic IOCG (iron-oxide–copper–gold) metallogenic province. Miner. Deposita 46 (7), 731–747.

Zhu, Z., 2016. Gold in iron oxide copper-gold deposits – A review. Ore Geol. Rev. 72, 37–42.

Editorial responsibility: N.N. Kruk